Supplementary Information (SI) for Nanoscale.

Supplementary Information: Local strain-engineering of exciton energy in 2D materials with nanoindentation

Kristyna Yang[1], Yucheng Yang[1], Daniel A. Rhodes[2], Katayun Barmak[2], Matthew R. Rosenberger[1]

[1]Department of Aerospace and Mechanical Engineering, University of Notre Dame, Notre Dame, IN 46556
[2]Department of Applied Physics and Applied Mathematics, Columbia University, New York, NY 10027

Broken Indent AFM topography and PL map:

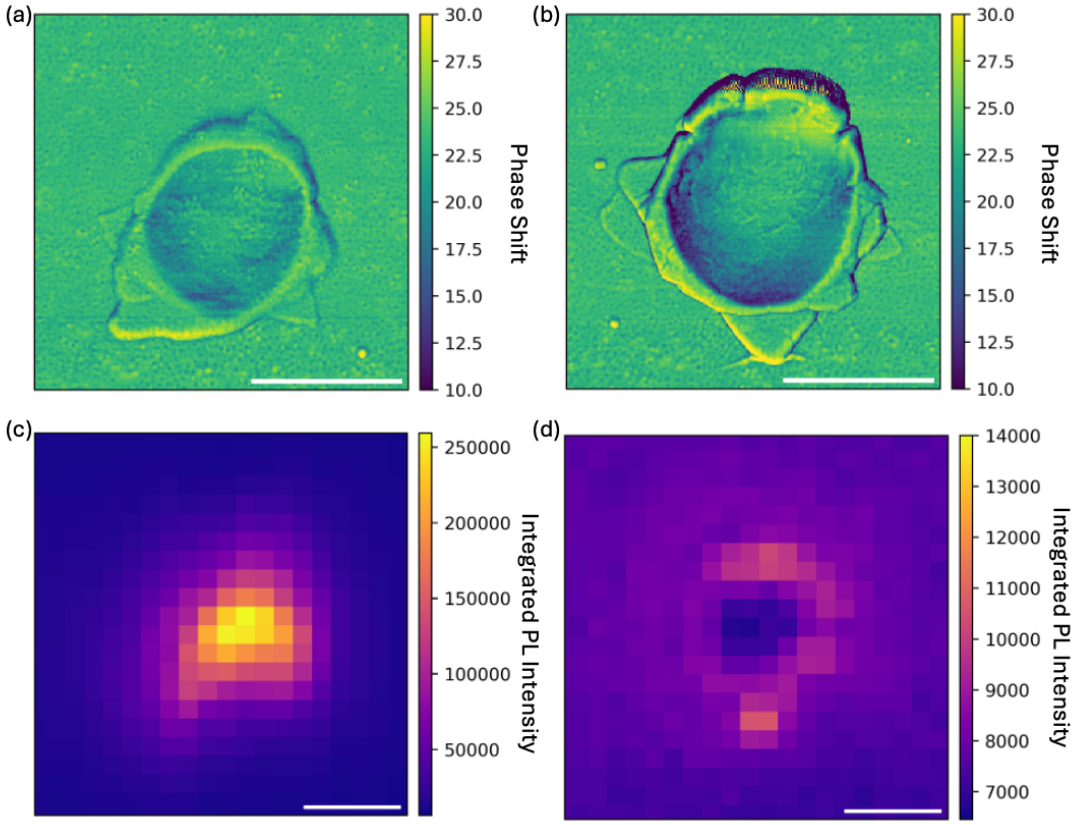

SM Figure 1 – (a) the Phase image of an unbroken, R = 1000 nm indent. (b) the Phase image of a broken R = 1000 nm indent. (c) and (d) PL integrated intensity of the indents in (a) and (b), respectively, over the red energy range described in Figure 3a. Scalebars in (a) and (b) are 1um. Scale bars in (c) and (d) are 2 um.

SM Figure 1 shows the phase component of the AFM topography data for a non-broken indent and a broken indent as well as the corresponding PL integrated intensity for each indent in the low energy range, the red shaded region in Figure 3a, 1.35 – 1.45 eV. The phase image of the broken indent, SM Figure 1b, shows faint lines on the inside of the indent which are not present on the inside of the unbroken indent in SM Figure 1a.

These lines indicate the broken edges of the WSe_2 material inside the indent. The broken nature of the WSe_2 material is further confirmed by the PL integrated intensity maps shown in SM Figure 1c and d. SM Figure 1c shows significant low energy emission from the bottom of the unbroken indent. SM Figure 1d shows an absence of low energy emission from the bottom of the broken indent. These metrics were used to determine the broken vs. unbroken state of indents for plots in Figures 1, 3, and 7.

Strained Indent Defect Introduction Experiment:

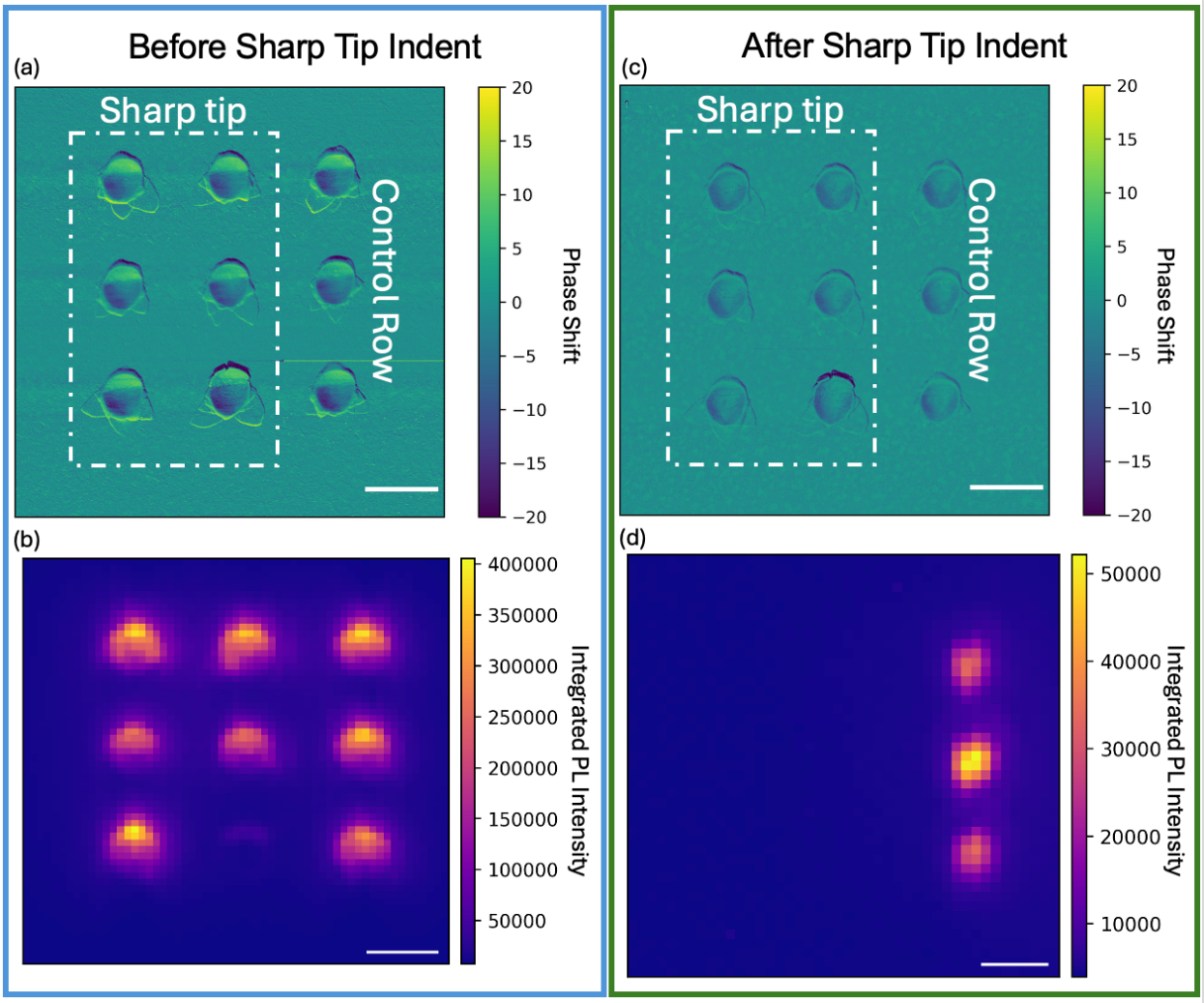

SM Figure 2 – AFM phase images (a,c) and corresponding low-energy integrated PL intensity maps (b,d) for a grid of identical indents (z = 3000 nm). (a,b) before and (c,d) after indentation with a sharp probe in the center. The dashed region indicates indents subsequently indented by the sharp tip, while the rightmost column was not indented with a sharp tip. All Scale bars are 1 um.

SM Figure 2 illustrates the effect of a small ML fracture on the optical response of strained ML WSe_2 indents. Initially, nine nominally identical R = 1000 nm indents were created with z = 3000 nm (of which eight remained unbroken). SM Figure 2a shows the phase image of all 9 indents and SM Figure 2b shows the corresponding Integrated PL Intensity map, in the red energy region. As evident in SM Figure 2a, the one broken

indent with faint lines in the phase image, has virtually no corresponding low energy emission (SM Figure 2b). Following the initial R = 1000 nm sphere tip indentation, and PL imaging, a sharp probe was used to introduce the smallest achievable, ML fracturing force into the center of the first six indents (left two columns of the indent grid), producing a minimal mechanical perturbation while locally fracturing the monolayer material. The minimum force required for ML WSe_2 fracture was found on a separate, unstrained region of the sample, and was identified by a noticeable decrease in force in the indentation (force vs. displacement) plot.

Following this indentation with a sharp tip, the AFM phase image, SM Figure 2c, shows subtle cracks at the bottom of the indents indented by the sharp tip, consistent with localized fracture of the WSe_2. The corresponding integrated PL intensity map, SM Figure 2d, shows a complete lack of low-energy emission from these indents, while the rightmost column of indents, which was not indented by the sharp tip, retains strong low-energy PL emission (note that SM Figure 2d imaging was conducted with a lower magnification objective thus the difference in overall intensity).

The simultaneous emergence of fracture patterns in the phase image and the disappearance of low-energy PL, indicate that even a minimal crack at the bottom of a strained indent is sufficient to cause full fracture and relaxation the locali strained ML. This result demonstrates that the relative absence of low-energy emission from indents is a reliable indicator of fracture and strain relaxation.

Laser spot size measurement:

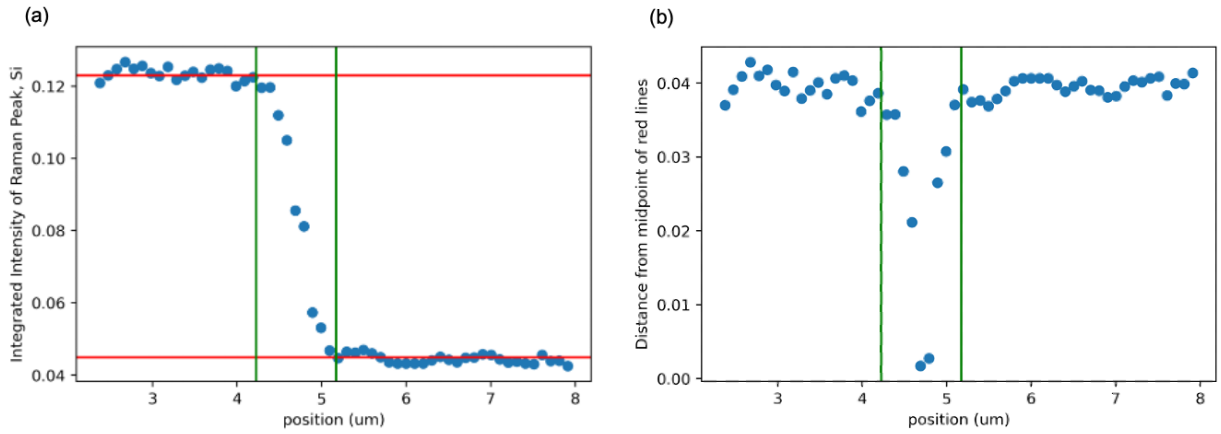

SM Figure 3 – (a) Raw data from the Si Raman peak measurement. Red lines indicate the mean of the data far away from the Au edge. Green lines indicate the x locations where the laser beam has started to cross and has finished crossing the edge. (b) absolute value of the data in (a) subtracted from the mean between the two red lines shows a gaussian beam intensity distribution.

The size of the laser spot was estimated using a knife edge measurement across a gold edge on a SiO2/Si wafer. The Si Raman peak height was measured in a straight

line across the edge of the gold at 0.1 um pixel spacing. The resulting data is shown in SM Figure 3. Based on the green line spacing the width of the laser spot is 0.95 um.

Cross Sectional Profiles of Indents:

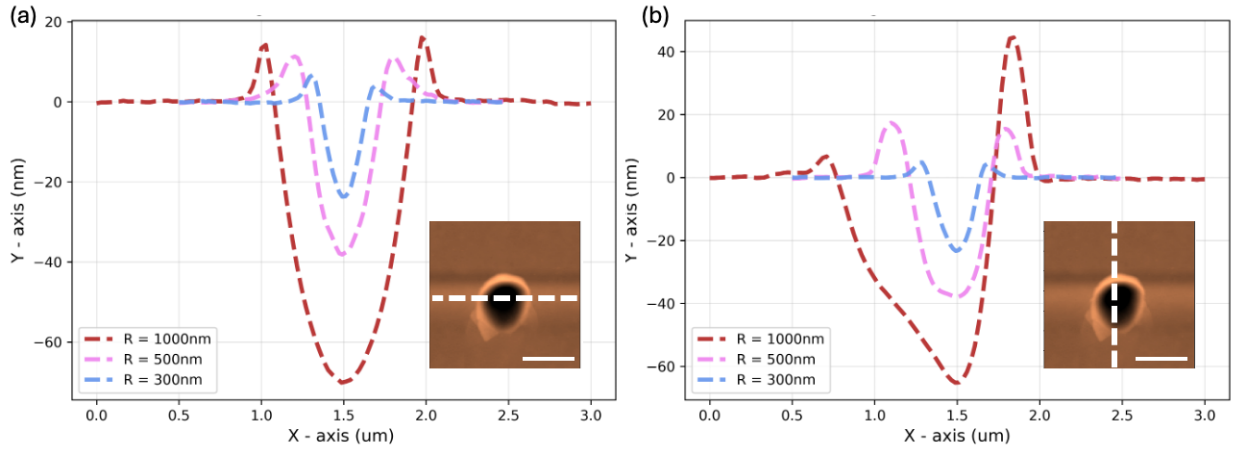

SM Figure 4 – Average AFM topography line profiles along the (a) x-direction and (b) y-direction for indents with similar aspect ratio (AR ≈ 0.080) produced using spherical tips of different radii (R = 1000 nm, 500 nm, and 300 nm). Insets show representative AFM topography images with the corresponding line-scan directions indicated.

To compare the line scans of indents produced with different tip radii, average AFM line profiles were extracted along orthogonal directions for indents with comparable aspect ratios. SM Figure 4a shows that, despite the large differences in tip radius, the overall indentation profiles exhibit similar qualitative shapes in the x-direction. However, in the y-direction, SM Figure 4b, the line scan of the larger, R=1000 nm tips are skewed towards the front end of the indent. The smaller R= 500 are less noticeably skewed, and the R = 300 nm indents profile appears nearly identical in shape to the x-line scan. We note that the x and y axes are not equal.

SM Figure 4b clearly illustrates the discrepancy in indent shapes which is discussed in the main text as the cause of higher intensity low energy PL emission on one side of the indent (the front end) than the other. The difference in the y-line scan shapes with R size supports the interpretation that larger indent radii require a larger force to displace the PS, which results in a forward sliding motion of the tip until enough PS has built up in front of the sphere tip to prevent further sliding, thus causing the forward skew of the R = 1000 nm indents.

Indent Fracture Statistics:

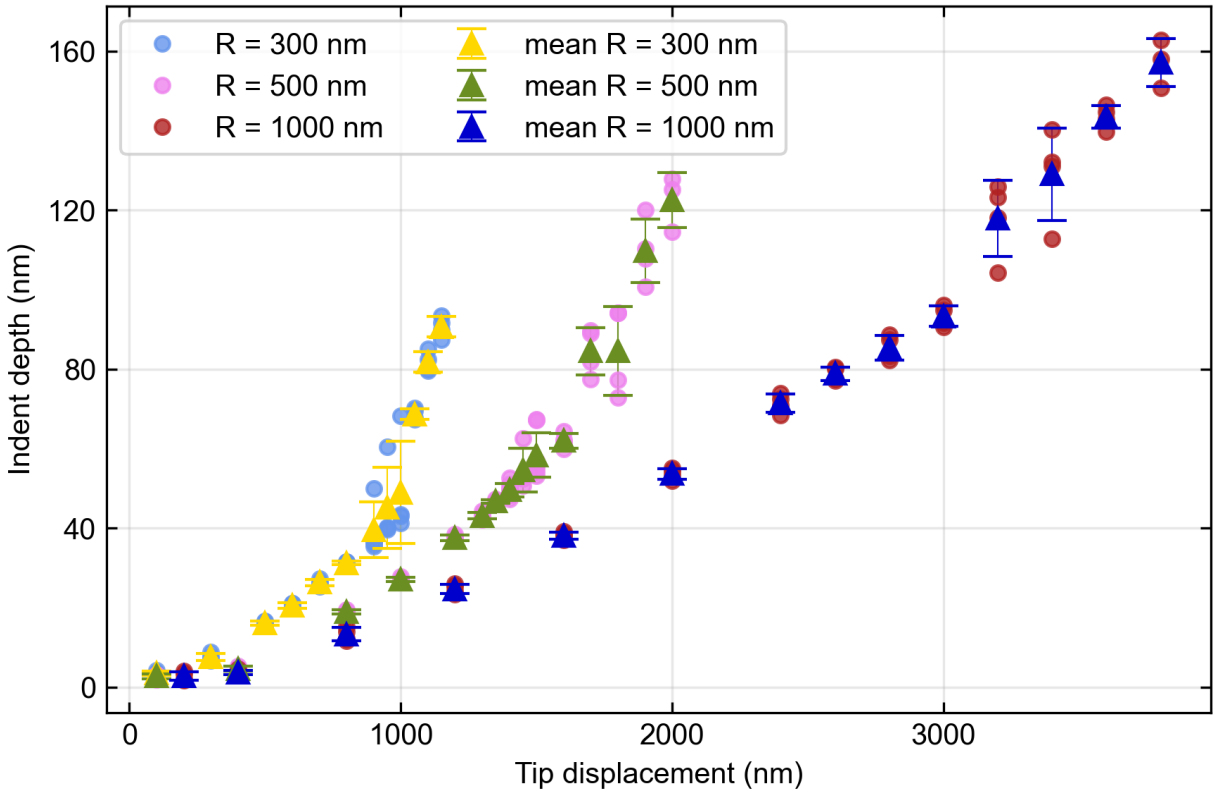

SM Figure 5 – a plot of the average indentation depths with error bars of 1 sigma for all data points in Figure 1b of the main text.

The datasets presented in Figures 1b and 7a are based on large grids of indents created using three different spherical tip radii. For each tip displacement magnitude, four nominally identical indents were produced. In total, these data sets include:

- R = 1000 nm, 55 indents
- R = 500 nm, 67 indents
- R = 300 nm 48 indents

(Odd numbers for R = 1000, and R = 500, because the last displacement in the data set, far past the breaking point, contains 3 indents instead of 4). These ensembles form the basis of the mechanical trends and breaking statistics discussed in the manuscript. However, the data presented in Figures 2, 5, and 7 are separate, smaller experiments which are not included in the following fracture statistics for simplicity.

Indent fracture is evaluated in the context of aspect ratio, rather than absolute depth or displacement. Below a critical aspect ratio, no fractures are observed for any tip radius. Above this threshold, fracture probability increases rapidly. For clarity, we

summarize the fracture statistics for the highest relevant displacement values (near the breaking regime) below:

SM Table 1

Tip Radius, R (nm)	Displacement, *z* (nm)	Unbroken/total
300	Displ = 900	3 /4
	Displ = 950	3 /4
	Displ = 1000	3 /4
500		
	Displ = 1500	2 /8
	Displ = 1600	4 /4
	Displ = 1700	0 /4
	Displ = 1800	2 /4
1000		
	Displ = 3200	1 /4
	Displ = 3400	1 /4

To more clearly evaluate the spread of data in all regimes, before fracture, at fracture, and beyond fracture, the mean indent depth for each z is plotted with error bars of one standard deviation in SM Figure 5. The mean and standard deviation were calculated from the multiple indents produced at each displacement. This plot corresponds directly to the datasets used in Figures 1b and 7a of the main text.

Unstrained Neutral Exciton Energy:

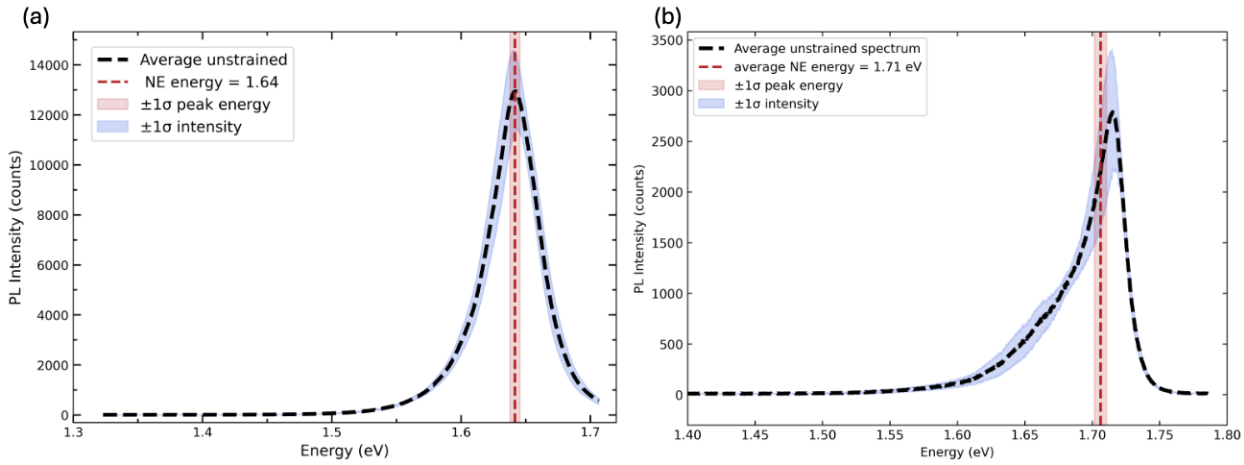

SM Figure 6 – Unstrained NE photoluminescence spectra at (a) RT and (b) 78 K. The black dashed curve shows the average unstrained PL spectrum obtained from multiple unstrained regions of the sample. The blue shaded region indicates the pointwise ±1σ variation in PL intensity. The red dashed line marks the mean NE peak energy extracted from Voigt fits to the individual spectra, with the red shaded region indicating the corresponding ±1σ confidence interval.

SM Figure 6(a) and (b) show the unstrained neutral exciton (NE) PL spectra at RT and at 78 K, respectively. For each plot, spectra were extracted from unstrained regions of several PL maps in our sample and averaged to obtain a representative unstrained PL line shape (black dashed curve). The shaded blue region indicates the pointwise ±1σ variation in PL intensity, reflecting within sample variation. Each individual unstrained spectrum was independently fit using a single Voigt function to extract the NE peak energy, and the resulting distribution of peak energies was used to compute the mean unstrained NE energy, the red dashed line, and its standard deviation, the red shaded region. These unstrained NE energies serve as the reference baseline for strain-induced peak shifts discussed in the main text

Finding indent aspect ratio:

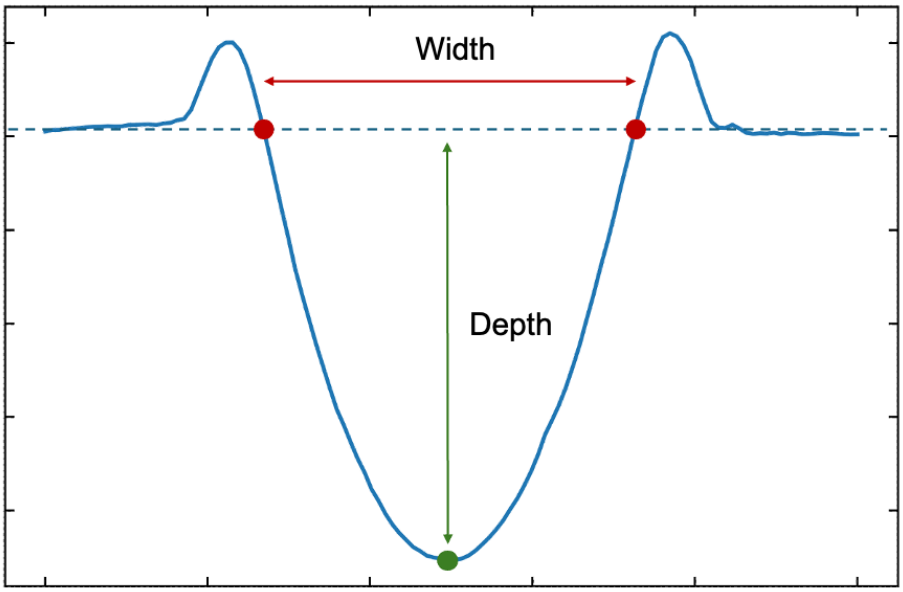

SM Figure 7 – Example line scan of an indent showing the definition of width and depth used for the aspect ratio calculation.

SM Figure 7 shows the definition of the depth and width used in the indent aspect ratio calculation. The line scan containing the deepest measured point in the indent is used for the calculation. The area outside the indent is set to zero and the depth of the indent is defined as the lowest point in the line scan relative to zero. The width is defined as the distance between the first two points on either side of the deepest point which are above zero.

Raman Imaging of Strained Indent:

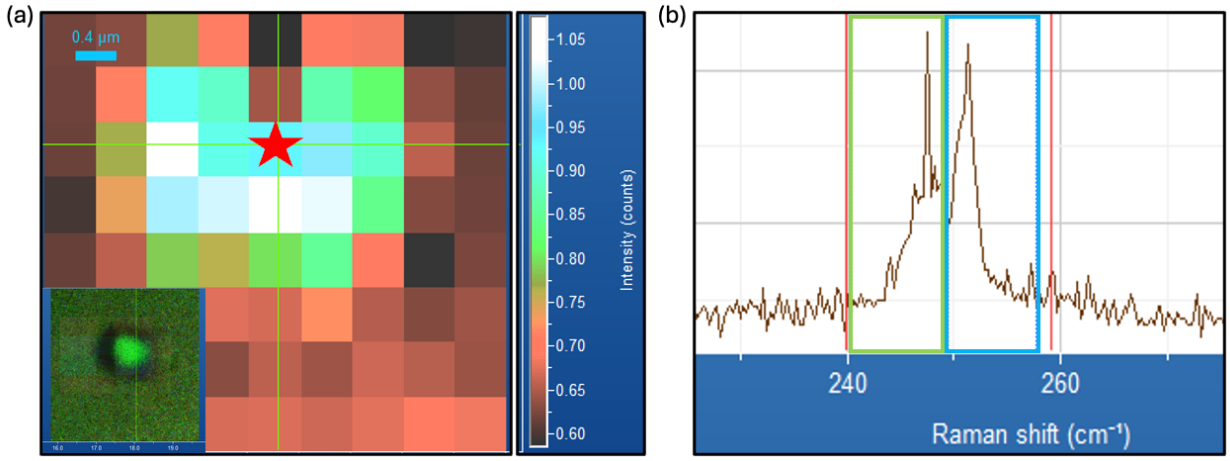

SM Figure 8 – (a) plot of an Integrated Raman Intensity ratio map which shows the ratio of the integrated intensities of the Green/ Blue regions in (b). Inset shows the optical image of the indent, (b) an example spectrum (location marked by red star in (a)) of a spectrum from (a) clearly showing a split in the E' Raman peak near the center of the indent.

Raman spectroscopy of our samples is complicated by the polymer substrate and limited signal-to-noise at the low laser powers required to avoid heating and damage of the substrate.

Nevertheless, we performed Raman measurements on strained indents, as shown in SM Figure 8. SM Figure 8a and b show an example Raman spatial ratio map, and an example Raman split spectrum from these experiments. SM Figure 8b shows a clear splitting of the in-plane E′ modes, consistent with strain-induced symmetry breaking. However, due to spectral resolution limits and the constraints on laser power, these measurements do not allow a reliable quantitative extraction of the absolute strain magnitude. We therefore do not use Raman data to calibrate strain.

Strain Estimate from PL shift:

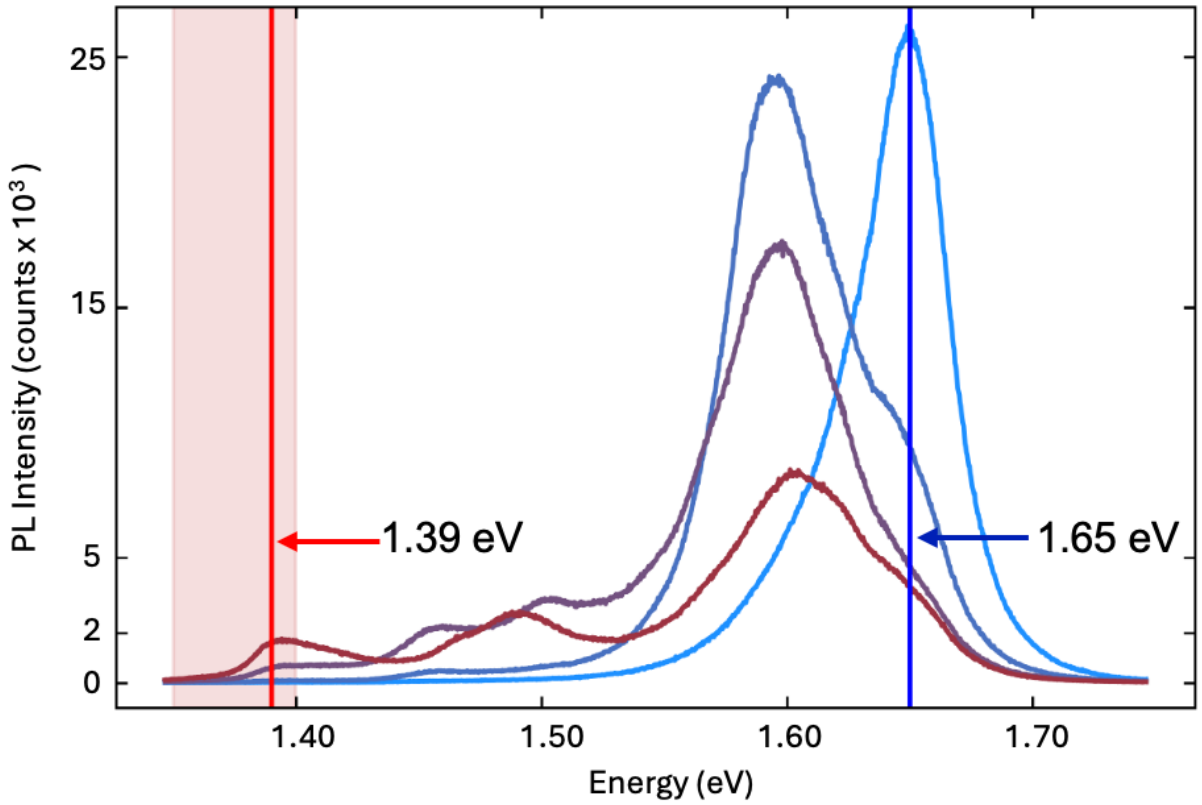

SM Figure 9 – Plot of spectral data of the indent shown in Figure 2a. Blue line is centered on the neutral exciton emission in a nearby, unstrained region. Red line estimates the location of the highest peak in the low energy emission range at the center of the indent.

SM Figure 9 illustrates the method used for estimating the strain % in our indents. The figure shows the same spectral data as in Figure 2b with a blue line at 1.65 eV marking the peak of the unstrained neutral exciton (light blue spectrum). The red line, at 1.39 eV, marks the approximate location of the peak furthest from the blue line, in the spectrum corresponding to the indent center (red spectrum). A previous study has reported the PL shift/strain % for several ML materials[2]. They reported a slope of $-109\ \mathrm{meV}/\%$ for a ML WSe2 exfoliated from a bulk crystal. Therefore, we use this slope to estimate the strain magnitude from the PL shift found in SM Figure 4, as shown in equation 2 below.

$$\varepsilon_{\mathrm{estimate}} = \frac{\text{PL shift}}{\text{slope}} = \frac{(1.64\ \mathrm{eV} - 1.39\ \mathrm{eV})}{0.109\,\frac{\%}{\mathrm{eV}}} = 2.29\ \%\ \mathrm{strain}$$